tvst

https://doi.org/10.1167/tvst.7.1.4

Article

The Interrelationship between Refractive Error, Blood Vessel Anatomy, and Glaucomatous Visual Field Loss

Mengyu Wang[1], Qingying Jin[1,2], Hui Wang[1,3], Dian Li[1], Neda Baniasadi[1], and Tobias Elze[1,4]

[1] Schepens Eye Research Institute, Harvard Medical School, Boston, MA, USA
[2] Jilin University, Changchun, China
[3] Jilin University of Finance and Economics, Changchun, China
[4] Max Planck Institute for Mathematics in the Sciences, Leipzig, Germany

Correspondence: Tobias Elze, Schepens Eye Research Institute, Harvard Medical School, 20 Staniford Street, Boston, MA 02114, USA. e-mail: tobias_elze@meei.harvard.edu

Received: 28 June 2017
Accepted: 1 November 2017
Published: 18 January 2018

Keywords: spherical equivalent; blood vessel location; retinal nerve fiber layer thickness norms; optical coherence tomography

Citation: Wang M, Jin Q, Wang H, Li D, Baniasadi N, Else T. The interrelationship between refractive error, blood vessel anatomy, and glaucomatous visual field loss. Trans Vis Sci Tech. 2018;7(1):4, https://doi.org/10.1167/tvst.7.1.4

Purpose: We quantified the interrelationship between retinal blood vessel (BV) anatomical variation, spherical equivalent (SE) of refractive error, and functional diagnostic parameters in glaucoma to identify optimal parameters for the improvement of optical coherence tomography (OCT) retinal nerve fiber layer thickness (RNFLT) norms.

Methods: A trained observer marked the intersections of the main superior/inferior temporal arteries and veins with concentric circles around the optic nerve head (ONH) center on fundus images. The interrelationship of BV, SE, and visual field global parameters was analyzed by multivariate regression and model comparison.

Results: A total of 445 eyes of 445 patients in a large glaucoma practice were selected. Of all investigated BV parameters, interartery angles (IAA) between superior and inferior arteries at a radius of 1.73 mm around the ONH center demonstrated the strongest relationship to SE (Bayesian information criterion difference to null model, 11.9). SE and BV parameters are unrelated to functional parameters, including mean deviation (MD), pattern standard deviation, and glaucoma hemifield test results.

Conclusions: BV locations outside the ONH are sufficiently stable over glaucoma severity to represent individual eye anatomy, and the IAA at 1.73 mm eccentricity is the optimal parameter to be considered for novel OCT RNFLT norms.

Translational Relevance: Among a large set of BV location parameters, considering IAA may improve RNFLT norms optimally and thereby increase the accuracy of clinical glaucoma diagnosis.

Introduction

Thinning of the retinal nerve fiber (RNF) layer (RNFL), which can be measured by optical coherence tomography (OCT),[1] is an important diagnostic criterion for glaucoma diagnosis and its progression. To support glaucoma diagnostics, OCT manufacturers provide normative databases and flag retinal areas on an individual RNFL thickness (RNFLT) measurement that deviate from these norms. However, there is a large interindividual variability of healthy RNFLT profiles due to anatomical variations between eyes.[2–4] So far, existing RNFLT databases only consider age but ignore the substantial variation of individual RNF bundle geometry. As a consequence, if individual nerve fiber bundles are located at a different retinal position than expected by the OCT machine, retinal locations on healthy eyes that are naturally thinner might be flagged abnormal by the OCT machine, whereas truly pathologic thinning of areas that are naturally thicker might be missed.[5,6]

One parameter readily available to clinicians, which represents the anatomical variations related to axial ametropia and is supposed to have a strong impact on individual RNF bundles, is spherical equivalent (SE) of refractive error.[7] It has been shown

that an adjustment of the measured RNFLT for individual refractive error can improve the detection of RNFL thinning in glaucoma.[8] However, following the rationale that the major diagnostic confounder is not refractive error but rather a deviation of the individual locations of the major RNF bundles, the diagnostic improvement should be considerably stronger when adjusting for RNF locations directly and interpreting RNFL thinning relative to the patient's individual RNF bundles. While individual RNF bundle locations can be determined by OCT for healthy eyes, the disease of glaucoma may result in progressive RNFL thinning, which may disguise predisease RNF bundle locations in glaucomatous eyes.

In contrast to predisease RNFL peak locations, major retinal blood vessels (BVs) are visible clearly and identifiable on fundus image regardless of glaucoma severity. Predisease local thickness maxima of the major RNF bundles, however, have been shown to be correlated strongly with major temporal artery and vein locations in the circumpapillary area,[9,10] as well as with vascularization density.[11] Moreover, it has been shown that taking individual artery locations on a single circle around the optic nerve head (ONH) into account considerably improved diagnostic performance of detecting RNFL defects.[6]

Before the development of a novel RNFLT database that takes BV locations and/or SE into account, it is necessary to investigate: (1) which type of major retinal blood vessels, that is, arteries or veins, are more relevant to represent individual eye anatomy, (2) which is the optimal eccentricity around the ONH to determine BV locations, and (3) how closely are BV locations and SE related to each other. Furthermore, to use BV locations as markers for predisease RNFLT peaks, it is an important premise that BV locations at the respective circumpapillary eccentricity do not substantially change with glaucoma progression. While BV location changes due to glaucoma have been observed within or, in case of smaller BVs, also in close proximity to the optic disc,[12–14] the relationship between glaucoma severity and major BV locations outside the optic disc to our best knowledge has not yet been studied systematically.

We aimed to lay the foundations for the generation of a novel RNFLT database by addressing the aforementioned issues. In particular, we determined major artery and vein locations on four concentric circles around the ONH and systematically studied the relationship between BV type and retinal location with SE as well as with glaucoma. Since there is an ongoing controversial discussion whether or how myopia could affect the structural diagnosis of glaucoma,[15–18] we based glaucoma diagnosis and severity on established functional diagnostic parameters.

Methods

This retrospective study was approved by the institutional review board (IRB) of Massachusetts Eye and Ear (MEE). The IRB waived the need for informed consent because of the retrospective nature of the study. The study adheres to the Declaration of Helsinki and all federal and state laws.

Subjects and Data Description

Circumpapillary ONH OCT scans and pairing visual fields (VFs; SITA Standard 24-2 protocol) of all patients who presented to MEE glaucoma service between 2011 and 2014 initially were selected and transferred electronically from the machines (Humphrey Field Analyzer HFA-II and Cirrus HD-OCT, Software version 6.5, Carl Zeiss Meditec AG, Jena, Germany). The data selection criteria for VF were fixation loss $\leq$ 33%, false-negative rates $\leq$ 20% and false-positive rates $\leq$ 20%. The data selection criteria for Cirrus OCT scan (Optic Disc Cube protocol with A-scan resolution 200 $\times$ 200 within an area of 6 $\times$ 6 mm) were signal strength $\geq$ 6 and within 1 year from the VF measurement. If more than one measurement per eye met the criteria, the most recent measurement was selected. If both eyes of a patient met the selection criteria, only one eye was included randomly to avoid potential bias of data samples. These initial preselection criteria resulted in 2161 eyes with paired OCT and VF measurements from 2161 patients.

Data Processing

The Cirrus OCT scan of ONH is centered around the optic disc with an area of 6 $\times$ 6 mm. The ONH center was determined by the Cirrus machine as the centroid of Bruch's membrane opening.[19] The retinal thickness color maps and corresponding fundus images of each eye were centered based on the ONH center. OCT scans with ONH centers that deviated more than 0.3 mm in horizontal and vertical direction from the fundus image center were excluded. To ensure the availability of data over the complete area

for each centered image, the edges of the centered images were removed by 0.3 mm, which resulted in an image area of 5.4 × 5.4 mm.

Missing data pixels were denoted by black areas on the retinal thickness color plot. We excluded the scans that had missing data in the temporal area of any of the four vessel tracking circles. In addition, all fundus images were inspected visually by a trained observer for motion artifacts due to eye movements during the scan. All scans with vessel displacements of at least one vessel diameter or visible displacements within the optic disc were excluded.

From HFA VF, we extracted summary parameters including mean deviation (MD), pattern standard deviation (PSD), and Glaucoma Hemifield Test (GHT). The SE of refractive error was extracted from the MEE medical records of the patients. A portion of the patients on the MEE glaucoma service were referred by external clinical institutions and their refractive error was not measured at MEE; therefore, those patients were excluded. Since cataract is a possible confounder as it may cause refractive errors related to the lens instead of eye anatomy, patients with cataract (nuclear sclerosis 3+ or worse) were excluded as well. For GHT, we only selected eyes with GHT outcomes that were related to glaucoma diagnosis, including within normal limits, borderline, and outside normal limits.

Vessel Tracking

For vessel tracking, we developed a custom software in the programming language R.[20] A trained observer marked the intersections of the major superior and inferior arteries and veins with four concentric circles with the radii 1.23, 1.73, 2.23, and 2.70 mm on each centered fundus image meeting our aforementioned data selection criteria, respectively. The graphic parameters on fundus images, such as the standard scanning circle or abnormality ratings, were switched off. Figure 1 shows an example of major superior and inferior artery intersections with the 1.73 mm circle.

We used the coordinate system of the Cirrus device, which defines the angular position of zero on the horizontal line towards temporal direction and calculate angles clockwise/counterclockwise for right/left eyes.

Statistical Analyses

All statistical analyses were performed by the R platform.[20] Generalized linear regression was applied to study the association between BV trajectory and SE and glaucoma diagnostic parameters. We performed multivariate linear regression for continuous parameters and logistic regression for noncontinuous parameters.

While linear regression models frequently are evaluated by null hypothesis significance tests based on P values, this approach has known limitations. First, nonsignificant P values cannot be interpreted as evidence against a parameter. Second, it does not provide a quantification of the strength of evidence of the parameters. Therefore, to assess which parameters truly are unrelated, as well as which parameter is closest related to BV locations or angles, we additionally applied an information theoretic model comparison approach based on the Bayesian Information Criterion (BIC).[21]

Our model comparison procedure is based on the following established rationale: Generally, if the slope parameter of the regression line is different from zero, then there is evidence that the corresponding input parameters are relevant to the output variable. We compared a model with the input parameters (hypothesis H_1) to a model without the input parameters (null hypothesis H_0 with zero slope). The model evidence of H_1 and H_0 was estimated by BIC, with lower BIC indicating higher model evidence. The BIC difference between H_1 and H_0 models was calculated. The sign of BIC difference implies which hypothesis is preferred and the absolute value of BIC difference represents the evidence difference between H_1 and H_0 models herein. We used the following established heuristic interpretation of the absolute value of BIC difference (Δ BIC): The evidence for a model is positive for $2 \leq \Delta$ BIC ≤ 6, strong for Δ BIC > 6, while for Δ BIC < 2, there is no substantial evidence for any of the two models H_1 and H_0.[22]

Results

Descriptive Statistics

Of 2161 eyes, 445 met the reliability criteria for data selection. Among the 202 male and 243 female patients, 214 were diagnosed with glaucoma and 231 were glaucoma suspects. Table 1 summarizes the demographic and diagnostic parameters of those patients. In addition, the GHT results of 228, 48, and 147 eyes were within normal limits, borderline, and outside normal limits, respectively.

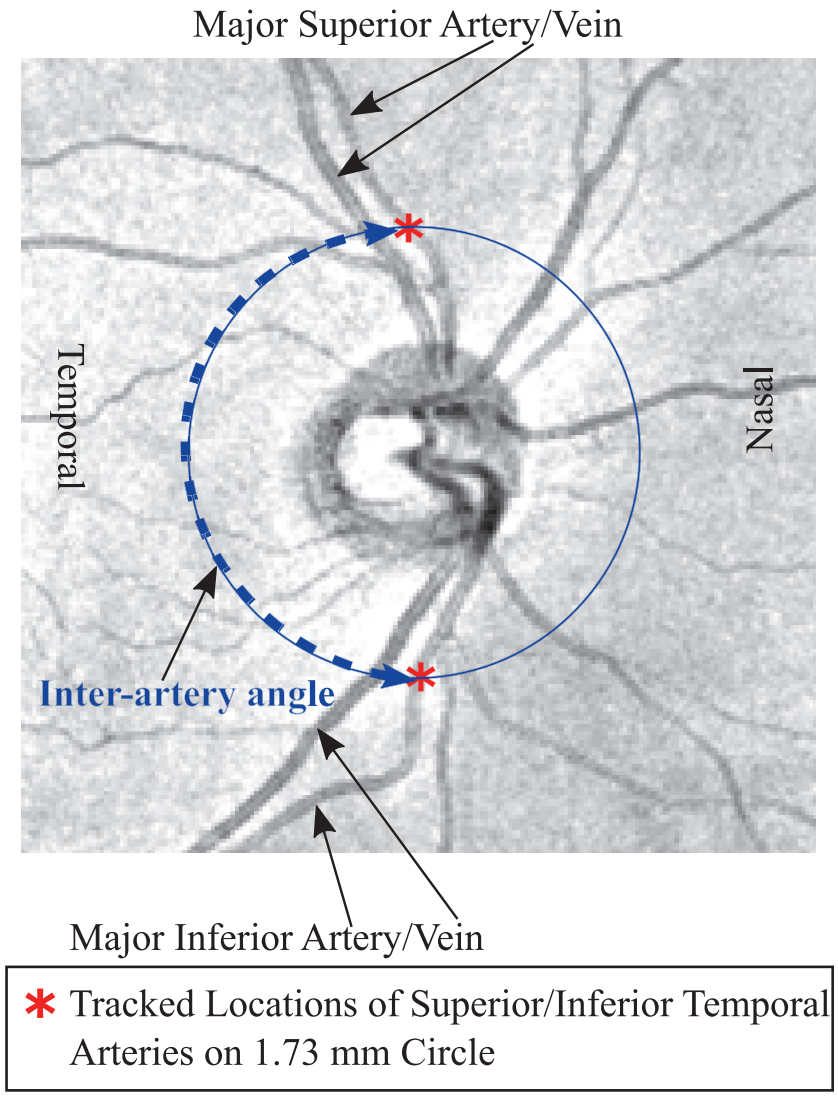

Figure 1. Example of fundus image of a right eye with tracked major superior and inferior artery locations on the 1.73 mm circle with respective interartery angles.

Relationship between BV Positions and RNFL Peaks

As for the 1.73 mm circle, normative RNFLT values were available through the Cirrus RNFLT color plots. We could specifically analyze the location differences between the BVs in our patients and the peaks of the RNFLT norms. Figure 2 illustrates that the mean BV locations were closely adjacent to the normative RNFLT peaks. Mean major superior arteries and veins were 2.93° and 5.18° ($P < 0.001$ for both) nasal to the superior RNFLT peak location, respectively. Mean major inferior arteries and veins were 2.35° ($P = 0.002$) temporal and 2.95° ($P < 0.001$) nasal to the normative inferior RNFLT peak location, respectively. Mean absolute angular differences between artery and RNFLT peak locations (10.75°) were significantly smaller ($P < 0.001$) than the mean absolute angular difference between vein and RNFLT peak locations (12.60°). Mean absolute angular

Table 1. Descriptive Statistics (Quantiles) of Patient Demographic and Glaucoma Diagnostic Parameters

Quantiles	Age	SE (Diopter)	MD (dB)	PSD (dB)
0%	16.4	−12.8	−32	0.9
25%	52.3	−2.5	−3.8	1.5
50%	60	−0.6	−1.9	1.8
75%	68.1	0.8	−0.5	2.8
100%	91.4	6.4	2	16.1

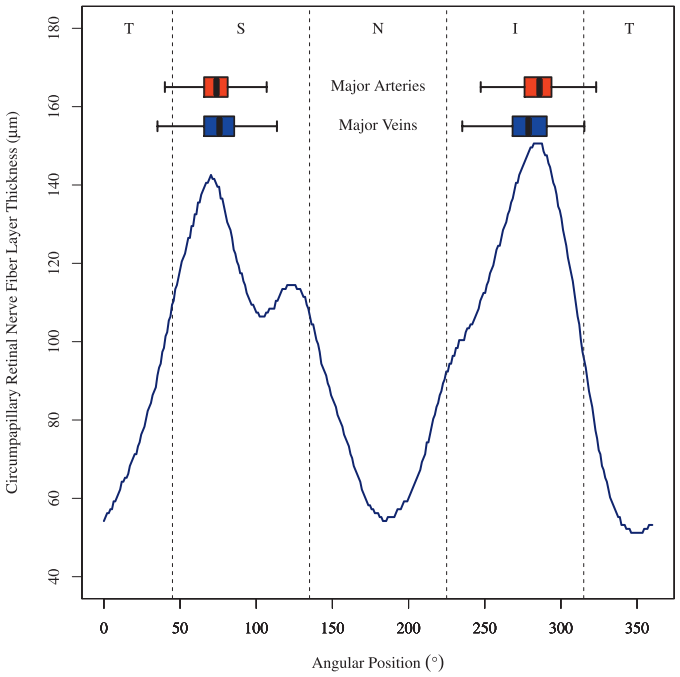

Figure 2. BV position distribution over all eyes on the Cirrus standard diagnostic circle with 1.73 mm radius. As a spatial reference, the Cirrus cpRNFLT norm was added (*blue line*). Here, the norm for the age of 52 years is shown. The absolute cpRNFLT values decrease with age, but the peak of Cirrus norms remains at the same location according to the Cirrus age model. *Boxplots*: distributions of BV locations (*box*: first to third quartile; *central mark*: median; *yellow point*: mean; *whiskers*: fifth to 95th percentile). *Dark red box*: artery locations, *dark blue box*: vein locations. T, temporal; S, superior; N, nasal; I, inferior with respect to the ONH.

differences between superior vessels and RNFLT peak locations (11.18°) were significantly smaller ($P < 0.02$) than the mean absolute angular difference between inferior vessels and RNFLT peak locations (12.17°).

Figure 3 shows illustrative examples of the superior RNFL peak location compared to superior artery and vein locations in patients with at most minimal VF depression (MD ≥ -1 dB) and advanced glaucoma (MD < -12 dB). In the example of patients with minimal VF depression, the superior artery and vein locations were 9.98° and 2.81° nasal to the superior RNFL peak location, respectively. For severe glaucoma, however, the distances were five to 13 times larger and in the opposite direction: The superior artery and vein locations were 52.69° and 37.70° temporal to the superior RNFL peak location, respectively.

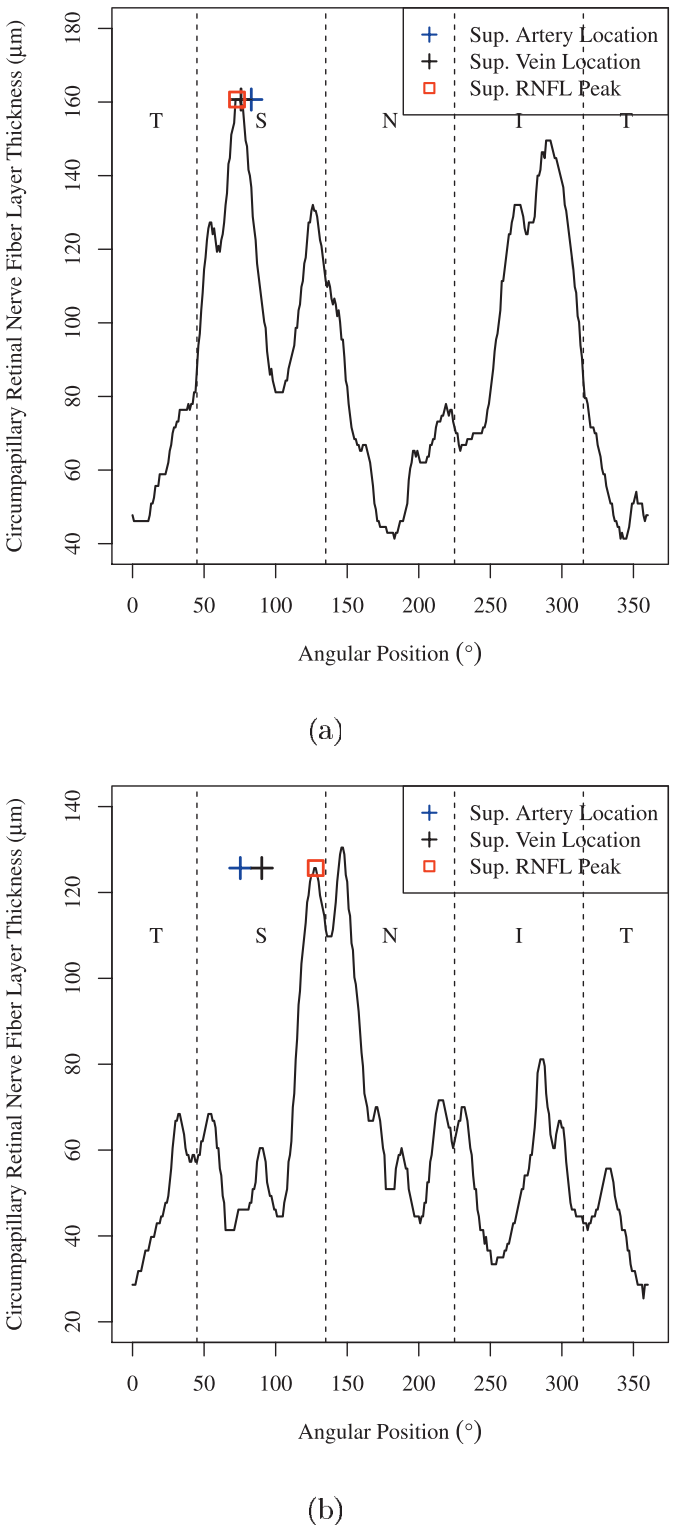

Figure 3. Illustrative examples of the superior RNFL peak location compared to superior artery and vein locations in (**a**) patients with minimal VF depression (MD ≥ -1 dB) and (**b**) patients with advanced glaucoma (MD < -12 dB).

BV Location Variations

Figure 4 shows the linear regression from (Fig. 4a) superior and (Fig. 4b) inferior artery and vein locations on the innermost circle (1.23 mm radius) to the the outermost locations (2.70 mm radius). All BIC differences are substantially greater than six, which indicates a very strong association between closest and farthest BV locations with respect to the ONH.

Figure 5 illustrates the decreased evidence for the associations between superior and inferior BV locations, from strong evidence for the two innermost locations to no evidence for the outermost location. The evidence of association between superior and inferior artery locations was stronger than the evidence for vein locations.

Relationship between BV and VF Parameters

Figure 6 shows the strength of evidence for the associations between superior/inferior (Figs. 6a, 6b) BV locations and VF summary indices and SE. There was no evidence that BV locations were associated with VF summary indices, including MD, PSD, and GHT outside normal limits. While there was strong/positive evidence that BV locations were associated with SE, the evidence of associations decreased with respect to the radial distance from the ONH. On average, the evidence of associations with SE was stronger for arteries than for veins and stronger for superior than for inferior BV locations. There was relatively consistent strong/positive evidence for the associations between BV locations and SE for the two smaller circles (radii, 1.23 and 1.73 mm) closer to the ONH.

Figure 7 shows the strength of evidence for the association between inter-BV angles and VF summary indices and SE. There was no evidence for associations between VF summary indices and inter-BV angles. SE was strongly/positively associated with inter-BV angles and the strength of association decreased with respect to the radial distance from the ONH. On average, interartery angles were stronger associated with SE than intervein angles. The evidence of the association between SE and the interartery angle on the Cirrus standard diagnostic circle (1.73 mm radius) was the strongest (BIC difference, 11.9) among all inter-BV angles, which also was much stronger than the strongest association (BIC difference, 8.4) between any of the single BV locations and SE shown in Figure 6.

Figure 8 shows the linear regression from SE to the

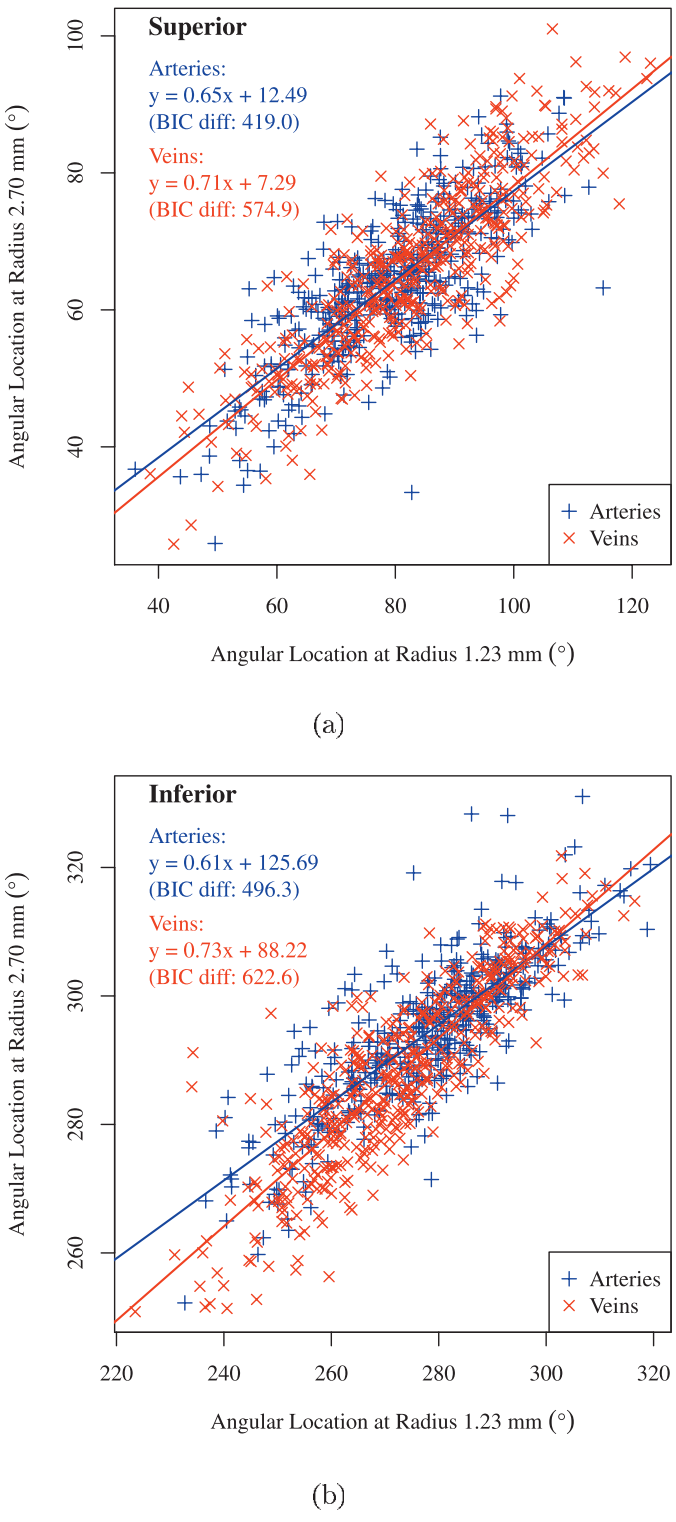

Figure 4. Linear regression of (**a**) superior and (**b**) inferior BV locations from the locations on the 1.23 mm circle to the locations on the 2.7 mm circle. *Blue*: arteries and *red*: veins. BIC Diff, difference of BIC.

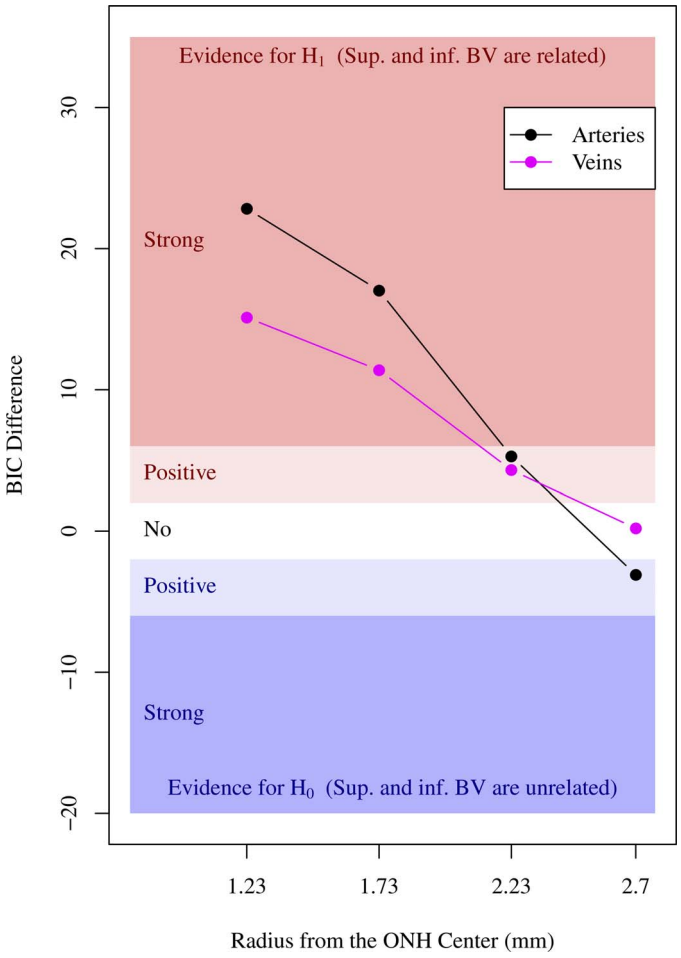

Figure 5. Strength of evidence for the association between superior and inferior BV locations on the four concentric circles around ONH (*black curve* with *circle point*: arteries and *magenta curve* with *square point*: veins). *Blue shaded area* indicated by the annotation "positive" and "strong" in the lower plot region below zero horizontal axis illustrates the area of evidence for the null hypothesis H_0 that superior and inferior BVs are unrelated. *Red shaded area* indicated by the annotation "positive" and "strong" in the upper plot region above zero horizontal axis illustrates the area of evidence for the alternative hypothesis H_1 that superior and inferior BVs are related. *White area* illustrates the area of evidence strength that both H_0 and H_1 models are not preferred over their counterpart alternative model.

interartery angles on the 1.73 mm circle compared to the linear regression lines for the relationship between SE and inter-RNFL bundle angles on the 1.73 mm circle in healthy myopic subjects from a previous study by Leung et al.[7] While the correlation between SE and inter-RNFL bundle angles in the latter study trended to be larger than the correlation between SE and the interartery angles in our study, this effect was not significant ($P = 0.15$).

Discussion

We found strong/positive evidence that decreasing SE values are associated with more temporal BV locations. Given the previously reported strong correlations between RNF bundles and major temporal artery locations,[9,23] these results are consistent with the previously reported decrease in RNF bundle angle with increasing myopia.[7] The evidence of association was stronger for arteries compared to veins, and stronger for superior compared to inferior BVs. In addition, in general, the evidence of associations decreased with increasing eccentricity from the ONH.

Notably, the inter-BV angles were stronger associated with SE than the single BV locations. This suggested that BV angles are more suitable anatomical markers for those effects of eye anatomy that are related to axial ametropia. Among all BV-related parameters, the strongest evidence for an association with SE was found for the interartery angle on the Cirrus standard circle (Fig. 6). This finding suggested that the interartery angle on the 1.73 mm circle would be the best candidate to be considered for novel normative RNFLT databases to address the numerous previously reported effects of myopia on the RNFLT profile.

While this conclusion is compatible with the previous finding that the angle between the two major RNF bundles was associated strongly with SE and axial length,[7] the interartery angle has the advantage of being easily detectable even in advanced glaucoma, whereas RNFLT peaks may change considerably due to glaucomatous RNFL thinning, as we illustrate in Figure 3. The tracked superior artery and vein locations were adjacent to the superior RNFL peak location in a patient with MD ≥ -1 dB, while there was a large discrepancy between the tracked superior BV locations and RNFL peak location in a patient with MD < -12 dB.

If the locations of major temporal BVs changed considerably in the course of glaucoma, their use as anatomical markers for patient-specific RNFL norms would be questionable. Glaucomatous BV location changes have been observed within or, in case of smaller BVs, also in close proximity to the optic disc.[12,13] Our model comparison results indicated that potential individual BV location shifts related to glaucoma severity (measured by MD, PSD, and GHT test results), are too small compared to the natural variation of BV locations to confound potential BV

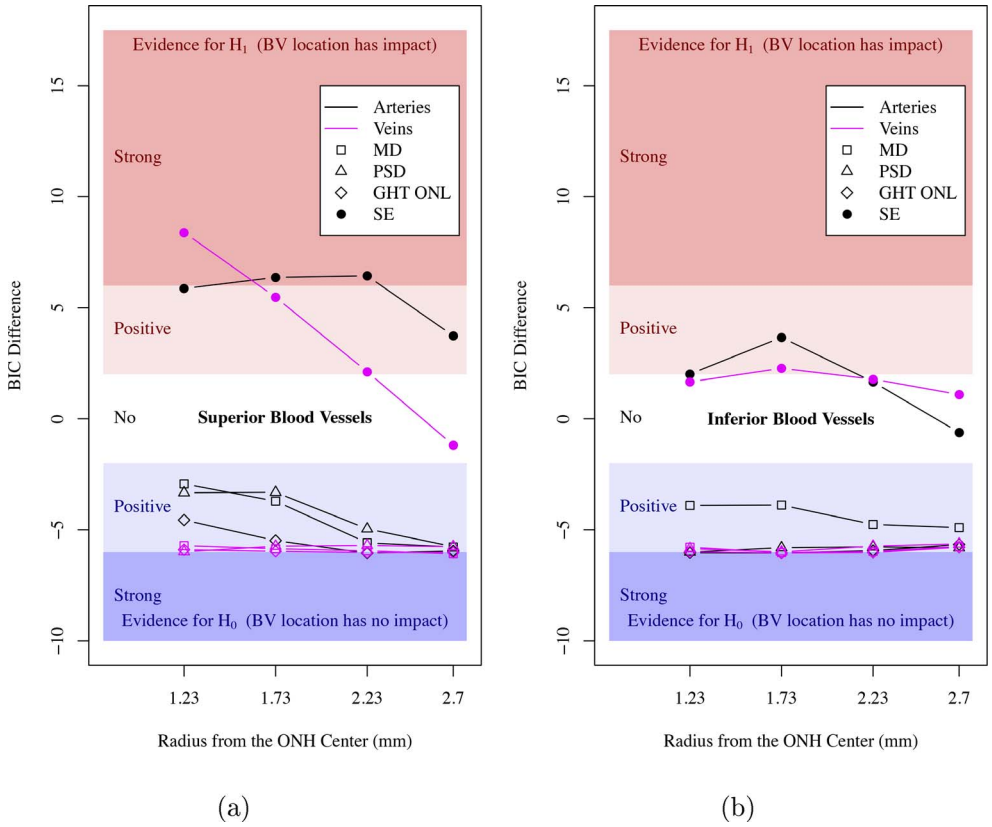

Figure 6. Strength of evidence for the association between superior/inferior (**a**, **b**) BV locations and VF summary indices (*open symbols*) and SE (*filled circles*) on the four concentric circles around ONH (*black curves*: arteries, *magenta curves*: veins). GHT ONL: glaucoma hemifield test outside normal limits.

location-specific norms (all BIC differences in Figures 6 and 7 are smaller than −2). While this does not rule out that individual BV shifts might occur and might be found in future longitudinal studies, our findings suggested that the locations of major BVs on the standard measurement circle are robust enough to be used as markers for retinal anatomy regardless of glaucoma severity.

The close relationship of the distributions of tracked BVs and the Cirrus RNFL thickness normative distribution (Fig. 2) is remarkable as our subjects are glaucoma patients, whereas the Cirrus RNFLT norms are based on 250 healthy controls,[19] which further indicated that BV locations remain stable under glaucoma. It has been argued previously that BVs themselves account for approximately 9% of the total RNFL area and, therefore, might contribute to a local overestimation of thickness at the BV locations, so that vessel regions should be subtracted from thickness.[24] However, it is unlikely that the close relationship of BV locations and RNFL thickness in our study is the result of such local overestimations, as arteries, which have lower diameters and, therefore, contribute less to RNFL area, are more closely related to the main RNF bundles than veins, which is confirmed by previous studies.[6,23]

While previous works[9,10] already demonstrated a relationship between vessel locations and RNFLT profiles, the main contribution of this work was to find the optimal vessel-related parameters as the markers of individual retinal anatomy to personalize RNFLT norms, which can contribute to a more personalized glaucoma diagnosis in future. To achieve this, we investigated a large set of vascular parameters in comparison, not only with respect to the optimal association with SE but also, equally important, with respect to their stability over glaucoma severity. This is a necessary prior condition to the establishment of novel normative data sets.

This study has limitations. While we have shown the impact of glaucoma on BV locations to be considerably smaller compared to the impact of SE and the natural variations of the individual eye anatomy, our cross-sectional data did not allow a

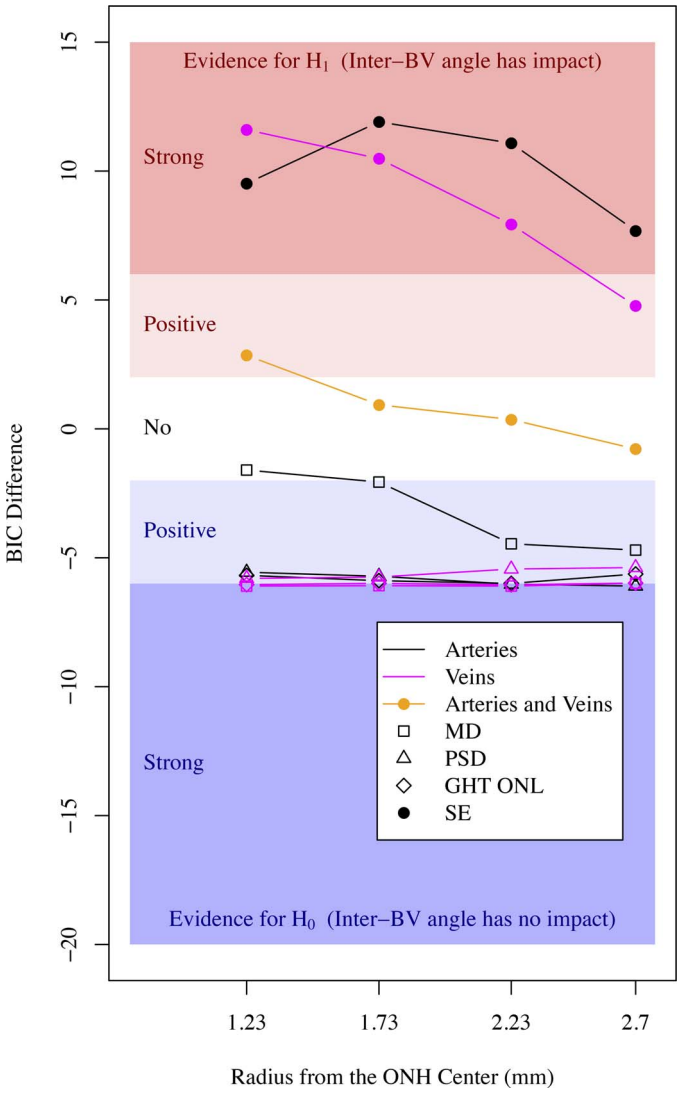

Figure 7. Strength of evidence for the association between inter-BV angles and VF summary indices (*open symbols*) and SE (*filled circles*) on the four concentric circles around ONH (*black curves*: arteries, *magenta curves*: veins). The *orange curve* denotes strength of evidence from intervein angles in addition to the evidence obtained from interartery angles.

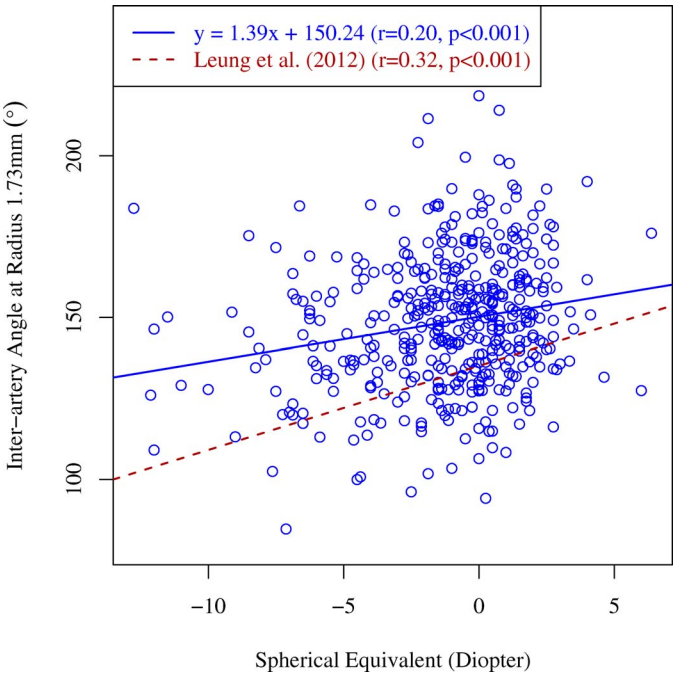

Figure 8. SE in diopters versus interartery angle in degrees on the circle with 1.73 mm radius around the ONH. *Solid blue line*: regression line. For comparison, the regression line characterizing the relationship between inter-RNFL bundle angle and SE in healthy myopic subjects from an earlier work by Leung et al.[7] (*dashed red line*) has been added.

detailed study of possible vessel shifts in individual eyes in the course of glaucoma progression. Detailed longitudinal studies might reveal subtle individual glaucomatous BV shifts that could be taken into account to improve the models introduced in this work. Furthermore, the determination of the interartery angle at the Cirrus standard circle, which proved to be the optimal parameter to represent anatomic changes due to axial ametropia, is not automatically extracted by OCT machines and must be tracked manually. However, given the clear visibility of the major temporal retinal blood vessels regardless of glaucoma severity, we expect that automated detection methods based on image processing could be developed easily by OCT manufacturers.

To conclude, individual eye anatomy has been reported repeatedly to confound the interpretation of OCT RNFLT measurements but currently is not considered by the norms included in the OCT machines. In contrast to individual RNF bundles, major blood vessels are detectable easily regardless of glaucoma severity. In this study, we systematically investigated which of the numerous blood vessel location parameters are most suitable to represent those anatomic variations among eyes that are assumed to have the strongest confounding effects on clinical OCT interpretations. Our results have a considerable translational potential as they indicate that the interartery angle on the 1.73 mm circle around the ONH would be the optimal parameter to be considered in novel normative RNFLT databases. The interartery angle may contribute to the future development of a more personalized glaucoma diagnosis, and its consideration also might improve

the understanding of specific VF loss from retinal structure.

Acknowledgments

The authors thank Peter J. Bex, Louis R. Pasquale, Lucy Q. Shen, Hiroshi Ishikawa, Joel Schuman, and Gadi Wollstein for their insightful suggestions to this work.

Supported by the Massachusetts Lions Foundation (MW, NB, TE), Grimshaw-Gudewicz Foundation (MW, NB, TE), Research to Prevent Blindness (MW, NB, TE), BrightFocus Foundation (MW, NB, TE), China Scholarship Council (HW) and NEI Core Grant P30EYE003790 (MW, NB, TE).

Disclosure: **M. Wang**, None; **Q. Jin**, None; **H. Wang**, None; **D. Li**, None; **N. Baniasadi**, None; **T. Elze**, None

References

1. Huang D, Swanson EA, Lin CP, et al. Optical coherence tomography. *Science*. 1991;254:1178–1181.
2. Amini N, Nowroozizadeh S, Cirineo N, et al. Influence of the disc–fovea angle on limits of rnfl variability and glaucoma discrimination. *Invest Ophthalmol Vis Sci*. 2014;55:7332.
3. Mwanza JC, Lee G, Budenz DL. Effect of adjusting retinal nerve fiber layer profile to fovea-disc angle axis on the thickness and glaucoma diagnostic performance. *Am J Ophthalmol*. 2016;161:12–21.
4. Choi JA, Kim JS, Park H, Park H, Park CK. The foveal position relative to the optic disc and the retinal nerve fiber layer thickness profile in myopia. *Invest Ophthalmol Vis Sci*. 2014;55:1419–1426.
5. Yoo YC, Lee CM, Park JH. Changes in peripapillary retinal nerve fiber layer distribution by axial length. *Optom Vis Sci*. 2012;89:4–11.
6. Rho S, Sung Y, Kang T, Kim NR, Kim CY. Improvement of diagnostic performance regarding retinal nerve fiber layer defect using shifting of the normative database according to vessel position. *Invest Ophthalmol Vis Sci*. 2014;55:5116–5124.
7. Leung CKS, Yu M, Weinreb RN, et al. Retinal nerve fiber layer imaging with spectral-domain optical coherence tomography: interpreting the RNFL maps in healthy myopic eyes. *Invest Ophthalmol Vis Sci*. 2012;53:7194–7200.
8. Kang SH, Hong SW, Im SK, Lee SH, Ahn MD. Effect of myopia on the thickness of the retinal nerve fiber layer measured by cirrus hd optical coherence tomography. *Invest Ophthalmol Vis Sci*. 2010;51:4075–4083.
9. Hood DC, Fortune B, Arthur SN, et al. Blood vessel contributions to retinal nerve fiber layer thickness profiles measured with optical coherence tomography. *J Glaucoma*. 2008;17:519–528.
10. Hood DC, Salant JA, Arthur SN, Ritch R, Liebmann JM. The location of the inferior and superior temporal blood vessels and interindividual variability of the retinal nerve fiber layer thickness. *J Glaucoma*. 2010;19:158–166.
11. Pereira I, Weber S, Holzer S, et al. Correlation between retinal vessel density profile and circumpapillary RNFL thickness measured with Fourier-domain optical coherence tomography. *Br J Ophthalmol*. 2014;98:538–543.
12. Varma R, Spaeth GL, Hanau C, Steinmann WC, Feldman RM. Positional changes in the vasculature of the optic disk in glaucoma. *Am J Ophthalmol*. 1987;104:457–464.
13. Radcliffe NM, Smith SD, Syed ZA, et al. Retinal blood vessel positional shifts and glaucoma progression. *Ophthalmology*. 2014;121:842–848.
14. Wang M, Wang H, Pasquale LR, et al. Relationship between central retinal vessel trunk location and visual field loss in glaucoma. *Am J Ophthalmol*. 2017;176:53–60.
15. Baniasadi N, Wang M, Wang H, Mahd M, Elze T. Associations between optic nerve head–related anatomical parameters and refractive error over the full range of glaucoma severity. *Transl Vis Sci Technol*. 2017;6:9–9.
16. Baniasadi N, Wang M, Wang H, Jin Q, Mahd M, Elze T. Impact of anatomical parameters on optical coherence tomography retinal nerve fiber layer thickness abnormality patterns. *Proc SPIE*. 2017;10045:100450P–1.
17. Kang SH, Hong SW, Im SK, Lee SH, Ahn MD. Effect of myopia on the thickness of the retinal nerve fiber layer measured by Cirrus HD optical coherence tomography. *Invest Ophthalmol Vis Sci*. 2010;51:4075–4083.
18. Budenz DL, Anderson DR, Varma R, et al. Determinants of normal retinal nerve fiber layer thickness measured by stratus OCT. *Ophthalmology*. 2007;114:1046–1052.

19. Carl Zeiss Meditec, Inc. *Cirrus HD-OCT User Manual*. Carl Zeiss Meditec, Inc., 2012.
20. R Core Team. R: A language and environment for statistical computing. Vienna, Austria; 2014. Available at: http://www R-project org. 2015.
21. Schwarz G. Estimating dimension of a model. *Ann Statist*. 1978;6:461–464.
22. Kass RE, Raftery AE. Bayes factors. *J Am Stat Assoc*. 1995;90:773–795.
23. Yamashita T, Asaoka R, Tanaka M, et al. Relationship between position of peak retinal nerve fiber layer thickness and retinal arteries on sectoral retinal nerve fiber layer thickness. *Invest Ophthalmol Vis Sci*. 2013;54:5481–5488.
24. Patel NB, Luo X, Wheat JL, Harwerth RS. Retinal nerve fiber layer assessment: Area versus thickness measurements from elliptical scans centered on the optic nerve. *Invest Ophthalmol Vis Sci*. 2011;52:2477–2489.